Published in final edited form as:
Biomaterials. 2009 May ; 30(13): 2507–2515. doi:10.1016/j.biomaterials.2009.01.007.

Homogeneous and organized differentiation within embryoid bodies induced by microsphere-mediated delivery of small molecules

Richard L. Carpenedo[a], **Andrés M. Bratt-Leal**[a], **Ross A. Marklein**[a], **Scott A. Seaman**[a], **Nathan J. Bowen**[b], **John F. McDonald**[b,c,d], and **Todd C. McDevitt**[a,d,*]

[a] The Wallace H. Coulter Department of Biomedical Engineering, Georgia Institute of Technology/ Emory University, Atlanta, GA, USA

[b] School of Biology, Georgia Institute of Technology, Atlanta, GA, USA

[c] The Ovarian Cancer Institute, Georgia Institute of Technology, Atlanta, GA, USA

[d] The Parker H. Petit Institute of Bioengineering and Bioscience, Georgia Institute of Technology, Atlanta, GA, USA

Abstract

Cell specification and tissue formation during embryonic development are precisely controlled by the local concentration and temporal presentation of morphogenic factors. Similarly, pluripotent embryonic stem cells can be induced to differentiate *in vitro* into specific phenotypes in response to morphogen treatment. Embryonic stem cells (ESCs) are commonly differentiated as 3D spheroids referred to as embryoid bodies (EBs); however, differentiation of cells within EBs is typically heterogeneous and disordered. In this study, we demonstrate that in contrast to soluble morphogen treatment, delivery of morphogenic factors directly within EB microenvironments in a spatiotemporally controlled manner using polymer microspheres yields homogeneous, synchronous and organized ESC differentiation. Degradable PLGA microspheres releasing retinoic acid were incorporated directly within EBs and induced the formation of cystic spheroids uniquely resembling the phenotype and structure of early streak mouse embryos (E6.75), with an exterior of FOXA2+ visceral endoderm enveloping an epiblast-like layer of OCT4+ cells. These results demonstrate that controlled morphogen presentation to stem cells using degradable microspheres more efficiently directs cell differentiation and tissue formation than simple soluble delivery methods and presents a unique route to study the spatiotemporal effects of morphogenic factors on embryonic developmental processes *in vitro*.

Keywords

Embryonic stem cells; Embryoid bodies; Microspheres; Retinoic acid

1. Introduction

Pluripotent embryonic stem cells (ESCs) are a renewable cell source for studies of embryonic development, regenerative medicine and *in vitro* diagnostics. ESCs, derived from

*Correspondence to: Todd C. McDevitt, Georgia Institute of Technology/Emory University, The Wallace H. Coulter Department of Biomedical Engineering, 313 Ferst Drive, U. A. Whitaker Building, Suite 2102, Atlanta, GA 30332-0535, USA. Tel.: +1 404 385 6647; fax: +1 404 894 4243. todd.mcdevitt@bme.gatech.edu (T.C. McDevitt).

the inner cell mass of the blastocyst stage of development [1–3], can be induced to differentiate via aggregation into multi-cellular spheroids referred to as embryoid bodies (EBs) [4]. Cells within EBs differentiate in response to a variety of environmental stimuli, including cell–cell adhesions, cell–matrix interactions [5], cytokines [6], growth factors [7], and small molecules [8]. Because the EB microenvironment is comprised of a complex mixture of these extracellular stimuli, differentiation within EBs is typically heterogeneous and spatially disorganized. Efforts to manipulate the EB environment and subsequent ESC differentiation have focused primarily on controlling media composition [7] and assembly of EBs using different culture methods [9]; however, precise control over the molecular milieu within the interior of EBs has not been achieved by such approaches [10].

During development, morphogens are secreted locally and presented to embryonic cells in a spatially and temporally controlled manner to direct appropriate differentiation and tissue formation [11–14]. *In vitro* strategies to deliver morphogenic factors to EBs, namely diffusion of supplemental media components, do not accurately replicate this process, with exogenous morphogens originating in the external fluid rather than within the cell spheroid. In addition, the diffusion of soluble factors into EBs may be restricted by the formation of an exterior shell composed of collagenous matrix and tight E-cadherin mediated cell–cell adhesions at the EB surface [15]. These fundamental challenges in morphogen presentation to ESCs limit the ability of EBs to accurately serve as controlled models of embryogenesis *in vitro* and perhaps limit the homogeneity of differentiated phenotypes that can be attained using EB differentiation methods. Engineering of biomaterials-based approaches has been used successfully to control the spatiotemporal presentation of morphogens to 3D assemblies of cells [16,17]. Thus, the use of biodegradable microspheres to deliver morphogens directly within EBs may enable production of more homogeneous populations of differentiated cells.

In this study, we describe the differentiation effects of spatially and temporally controlled presentation of morphogenic factors to ESCs comprising EBs from degradable biomaterials. Microsphere incorporation within EBs was assessed as a function of initial mixing conditions, and the release and cellular uptake of a fluorescent dye from incorporated microspheres were evaluated. The morphology, gene and protein expression, and ultrastructure of EBs containing retinoic acid (RA)-loaded poly(lactic-*co*-glycolic acid) (PLGA) microspheres are reported. These studies demonstrate that biomaterials can be used to engineer the microenvironment within EBs to efficiently direct ESC differentiation, which may be applied in regenerative cell therapies, *in vitro* pharmaceutical screening and models of developmental biology.

2. Materials and methods

2.1. Microsphere fabrication

PLGA (50:50, Absorbable Polymers International) microspheres were fabricated using a water-in-oil single emulsion, as described [18]. Briefly, 200 mg PLGA was dissolved in dichloromethane (DCM) containing 50 μg CellTracker Red (Molecular Probes, Invitrogen Corp., Carlsbad, CA) or 600 μg RA (all trans, Acros Organics, Geel, Belgium), added to 0.3% PVA, and homogenized at 3000 rpm (Polytron PT 3100, Kinematica Inc., Bohemia, NY). DCM was evaporated for 4 h and microspheres were collected by centrifugation, washed with dH_2O, and lyophilized for 1–2 days (Freezone 4.5, Labconco, Kansas City, MO).

2.2. Cell culture

ESCs (D3 line) [4] were maintained in an undifferentiated state on gelatin-coated tissue culture plates in LIF-containing media as described previously [19]. EBs were formed from 2×10^6 ESCs inoculated in LIF-free media and cultured under rotary conditions [19]. EBs containing microspheres were produced by coating CellTracker Red or RA-loaded microspheres in 0.1% gelatin solution for 3 h prior to mixing with ESCs in various microsphere to cell ratios and a range of rotary speeds. EB media was exchanged every 1–2 days as needed. EBs were treated with 0.1 μM RA in DMSO between days 2 and 6 as a soluble RA treatment control.

2.3. Microsphere characterization

Initial CellTracker Red (CTR) loading in PLGA microspheres was determined by hydrolyzing microspheres in 0.1 M NaOH containing 5% SDS solution overnight, analyzing the solution with a fluorescent plate reader (SpectraMax M2^e, Molecular Devices, Sunnyvale, CA), and comparing relative fluorescence to a standard curve of CTR constructed under equivalent conditions; unloaded microspheres served as a blank. A CTR release profile was constructed over the course of 14 days by incubating CTR microspheres in PBS under light mixing, centrifuging the microspheres at various time points, and collecting and analyzing the supernatant in a fluorescent plate reader. Values were reported as the percent of initially loaded CTR released. RA release was characterized under the same conditions by hydrolyzing centrifuged microspheres in 0.1 M NaOH/5% SDS and analyzing this solution spectrophotometrically at 355 nm.

2.4. Quantification of microsphere incorporation in EBs

EBs containing CTR microspheres were collected after 2 days, counted, and lysed in 0.1 M NaOH/5% SDS solution overnight at 37 °C. The lysate was analyzed with a fluorescent plate reader, and the number of microspheres per EB was calculated using a standard curve constructed with a known number of microspheres hydrolyzed in NaOH/SDS solution.

2.5. Histology

Between days 6 and 10 of differentiation, EBs were collected, fixed in 10% formalin, embedded in Histogel (Richard–Allan Scientific), processed and paraffin embedded, as described [19]. Paraffinized samples were cut into 5 μm-thick sections, placed on glass slides and deparaffinized before staining with hematoxylin and eosin (H&E) or immunofluorescence. Prior to immunostaining, slides were subjected to 15 min pressure-cooker treatment in 10 mM citrate buffer. Samples were then permeabilized and blocked in 0.05% Triton X-100/2% BSA for 30 min, incubated with FoxA2 primary antibody (Santa Cruz Biotech., 1:400) in 2% BSA solution overnight at 4 °C, rinsed with PBS (3 × 5 min) and incubated with Alexa Fluor 488-conjugated secondary antibody (donkey-anti-goat, Molecular Probes) for 1 h. Slides were counterstained with Hoechst, mounted, cover-slipped and imaged using a Nikon 80i microscope (Nikon Inc., Melville, NY). For whole-mount EB immunofluorescence, EBs were washed in PBS, fixed for 1 h in 4% paraformaldehyde at 4 °C, and washed again 3 times in wash buffer (150 mM NaCl, 1 mg/mL bovine serum albumin, 0.1% Tween-20, 50 mM Tris). EBs were permeabilized for 30 min in 2% TritonX-100, re-fixed in 4% paraformaldehyde for 15 min, and then blocked in wash buffer for 1–3 h. Samples were incubated in Oct4 primary antibody (Santa Cruz Biotech.) overnight at 4 °C, washed again (3 times, 15 min), and then incubated in an FITC-conjugated goat anti-rabbit secondary antibody (Southern Biotech.) for 4 h at 4 °C. EBs were then stained with Alexa Fluor 546 phalloidin (1:40, Molecular Probes) and Hoechst (1:100). Finally, samples were re-suspended in a low volume of PBS and imaged with a Zeiss LSM 510 Confocal Microscope (Carl Zeiss Inc.).

2.6. Quantitative PCR

After 2, 4, 7 and 10 days, RNA was extracted from EBs with an RNeasy Mini kit (Qiagen Inc, Valencia, CA), converted to complimentary DNA (iScript cDNA synthesis kit, Bio-Rad, Hercules, CA), and analyzed using real time PCR (MyIQ cycler, BioRad) as described [19].

2.7. Affymetrix microarray

Total RNA was extracted from day 10 EBs containing unloaded microspheres and RA-loaded microspheres using an RNeasy Mini kit (Qiagen). Labeled cRNA from 3 μg of total RNA was generated using the One-Cycle Target Labeling and Control Reagents Kit (Affymetrix Inc., Santa Clara, CA) and hybridized to the Mouse Genome 430 2.0 Array according to manufacturer's protocols (Affymetrix). CEL files generated by the Affymetrix GeneChip Operating System (GCOS) were converted to expression level values using the affy and GCRMA packages of the Bioconductor project (www.bioconductor.org) for the R statistical programming environment (www.rproject.org). After GCRMA preprocessing, SAM [20] (Significance Analysis of Microarrays v.3.02) analysis was performed on the probe sets with log 2 intensity values ≥5.0 in at least one of the experimental replicates using the following relevant parameters: Delta = 1.35, minimum fold change = 3, number of permutations = 500, and False Discovery Rate = 0%. SAM yielded 1270 significantly differentially expressed probe sets (DEPs) between the RA treated and untreated EBs. These probe sets were filtered to exclude non-existent and redundant Gene Titles by Affymetrix Annotation (file Mouse430_2 Annotations, CSV format (13 MB, 3/19/08)), to produce 1057 differentially expressed genes (DEGs). The log 2 expression values for the 1057 DEGs were normalized by *Z*-score calculation and used to generate the heat map for presentation using Spotfire DecisionSite 9.1.1 (http://spotfire.tibco.com). Microarray data were deposited at the Gene Expression Omnibus website (http://www.ncbi.nlm.nih.gov/geo/) under accession GSE12333.

2.8. Scanning electron microscopy

Samples were fixed in 2.5% glutaraldehyde (Electron Microscopy Sciences) diluted in sodium cacodylate buffer (Electron Microscopy Sciences) for 1 h. After rinsing, samples were further treated in 1% osmium tetroxide (Electron Microscopy Sciences) for 1 h. Samples were dehydrated in graded acetone dilutions and critically point dried using a Polaron E3000 critical point dryer (Quorum Technologies Inc., Guelph, ON, Canada). Samples were sputter coated for 120 s at 2.2 kV using a Polaron SC7640 sputter coater and imaged using a Hitachi S-800 scanning electron microscope (Hitachi High Technologies, Pleasanton, CA).

2.9. Statistical analysis

Values are reported as mean ± standard deviation ($n = 3$). Statistical significance was determined using one or two way ANOVA coupled with Tukey's post hoc analysis using Systat (v12, Systat Software Inc.).

3. Results

3.1. Microsphere incorporation within EBs

Single cell suspensions of ESCs cultured in rotary suspension aggregated into spheroids in <24 h, and the resulting EBs developed a smooth, spherical appearance after ~4 days of differentiation [19]. Scanning electron microscopy (SEM) revealed the formation of a smooth, epithelial cell layer on the surface of day 10 EBs (Fig. 1A). Cross-sectional views of bisected EBs revealed the formation of an exterior layer approximately 10 μm thick

enveloping the entire EB (Fig. 1B, C). The appearance of a relatively dense shell-like layer suggested that the diffusion of soluble factors into EBs may be restricted, thereby limiting the exposure of cells in the EB interior to supplemental morphogens in the media as well as diffusion of molecules out of the EB, leading to entrapment of secreted factors and metabolic by-products within EBs.

Fluorescent PLGA microspheres were fabricated using a single emulsion method and characterized using SEM and fluorescent microscopy. Microspheres displayed a smooth and spherical morphology (Supplemental Fig. 1A) with an average diameter of 7.8 ± 1.8 μm (Supplemental Fig. 1B), and efficiently incorporated fluorescent molecules such as FITC (not shown) or CellTracker Red™ (Supplemental Fig. 1C). In order to incorporate microspheres within the interior of EBs, ESCs were mixed at a 2:1 ratio of gelatin-coated PLGA microspheres-to-cells. The small, spherical particles were clearly distinguished from the cells in transverse SEM views of EBs (red arrows, Supplemental Fig. 2), and clusters of microspheres were distributed throughout the interior of EBs. The spatial distribution of microspheres incorporated within EBs was assessed by confocal microscopy. After 2 days, EBs containing CellTracker™ Red-labeled microspheres were counterstained with CellTracker™ Green prior to imaging. Labeling was limited to the outermost 1–2 cell layers (Fig. 1D–F) of most EBs, which, together with observations from SEM images (Fig. 1B, C), indicated that the shell-like EB exterior impeded diffusion of molecules into the interior. In contrast, red microspheres appeared at all focal planes within the EBs, demonstrating that microspheres were distributed throughout the entire depth of the EBs.

To evaluate the ability to control microsphere integration within EBs, the extent of microsphere incorporation was examined as a function of initial mixing parameters. Gelatin-coated Cell-Tracker™ Red microspheres were mixed with ESCs at a range of microsphere to cell ratios (1:2, 2:1, 5:1) and various rotary mixing speeds (25, 40, 55 rpm). Differences in microsphere incorporation for the different speeds and mixing ratios were observed using fluorescent microscopy (Fig. 1G–I) and quantified using fluorescent spectroscopy of lysed EBs (Fig. 1J). Higher microsphere to cell ratios and slower rotary speeds were found to facilitate greater microsphere incorporation within EBs. However, normalizing microsphere incorporation to average EB volume demonstrated that EBs formed at 25 rpm (slowest speed and largest EBs) had the lowest level of incorporation, while EBs formed at 40 rpm had the highest incorporation (data not shown), indicating that the greatest microsphere density within EBs was achieved at 40 rpm. Importantly, microsphere incorporation did not appear to negatively impact EB growth, as EBs containing microspheres remained similar in size and morphological appearance as untreated EBs throughout differentiation (Supplemental Fig. 3).

3.2. Molecule release within EBs

Small molecule release from microspheres within the EB interior and uptake by cells were investigated using CellTracker™ Red loaded PLGA microspheres. Labeled microspheres were incorporated in EBs, and after three days of differentiation, the microspheres appeared largely as individual, punctate fluorescent spheres, with some diffuse fluorescence in the vicinity of the microspheres (Fig. 2A–C). In contrast, after 10 days of culture, individual microspheres exhibited reduced fluorescent intensity, and many of the EBs displayed uniform fluorescence throughout the cell aggregate (Fig. 2D–F). The fluorescent intensity profile across a day 3 EB contained multiple peaks (dashed line, Fig. 2C), corresponding to the presence of individual microspheres, whereas day 10 EBs exhibited uniform fluorescence throughout an entire cell aggregate (Fig. 2G), suggesting CellTracker was released from microspheres and taken up by cells. CellTracker release from microspheres incubated in PBS was triphasic (Fig. 2H), consisting of a burst phase (up to 24 h), sustained release (1–7 days) and a plateau region (7–14 days), where the rate of release decreased as

CellTracker availability diminished. After 3 days, (black arrow) <60% of CellTracker was released from microspheres, whereas >90% release was observed after 10 days (red arrow), indicating that CellTracker release was nearly complete before uniform fluorescence was exhibited in day 10 EBs. Collectively our results indicate that delivery vehicles incorporated within EBs present small molecules locally to cells throughout the entire aggregate. Additionally, these results suggested that microsphere-mediated delivery within EBs distributed molecules more uniformly to cells in EBs than traditional soluble treatment methods, which are limited by diffusional barriers created at the exterior surface of EBs.

3.3. Retinoic acid delivery

Using the above method we examined ESC differentiation in response to microsphere-mediated delivery of a small molecule morphogen. Retinoic acid (RA), a derivative of vitamin A important in regulating embryonic development [21], was encapsulated in microspheres (3 μg RA/mg PLGA, with release profile in Supplemental Fig. 1D) and mixed with ESCs to form EBs. EBs treated with soluble RA (0.1 μM, days 2–6) or unloaded microspheres as well as untreated EBs served as controls. At early time points, EBs containing RA microspheres (RA MS EBs) appeared smaller than the other treatment groups, though after 6 days, RA MS EBs appeared noticeably larger than other EBs. After 10 days of differentiation, the RA microsphere-containing EBs exhibited a dramatically different morphologies than controls. While untreated (Fig. 3A) and soluble RA (Fig. 3C) treated EBs were solid spheroids, EBs containing unloaded microspheres displayed small void spaces (Fig. 3B) and EBs with RA microspheres formed large cystic structures that comprised the majority of the EB (Fig. 3D). Small cystic regions were observed in 90.0 ± 4.0% of RA MS EBs, compared to 29.1 ± 11.5%, 9.7 ± 2.3% and 5.6 ± 7.9% for unloaded MS, soluble RA and untreated EBs, respectively (Fig. 3I). Completely cystic EBs, which consisted entirely of the two epithelial layers, were found in 30.6 ± 12.7% of RA MS EBs, compared to <1% for all other treatment groups. Upon inspection at higher magnification, the bilayer morphology of cystic EBs consisted of a flattened endoderm-like cell population (red arrows, Fig. 3G, C, H) enveloping a pseudo-stratified columnar epithelial cell layer (black arrows, Fig. 3G, H). Higher concentrations of soluble RA (≥10 μM) did not induce formation of cystic EBs and instead resulted in formation of fewer, smaller EBs, while lower RA concentrations (≤10 nM) resulted in EBs similar in appearance to untreated spheroids, indicating that morphological differences between RA MS and soluble RA EBs were not solely attributed to differences in RA concentration (Supplemental Fig. 4A–C). Similarly, microspheres containing higher levels of RA (30 μg RA/mg PLGA) reduced EB size and microspheres with less RA (0.3 μg RA/mg PLGA) exhibited fewer cystic EBs, indicating a dose dependent response to microsphere-mediated RA delivery (Supplemental Fig. 4D–E). The formation of cysts in RA MS EBs took place over the course of ~4 days, with multiple small cystic regions appearing within EBs after 6 days of differentiation (Supplemental Fig. 5s). By 8 days, individual cysts were noticeably larger within EBs containing RA-releasing microspheres, and complete cavitation occurred by 10 days of differentiation, indicating that the continuous columnar layer of cells arose from the progressive merger of the smaller cystic structures.

3.4. Gene expression analysis

Based on the significant differences in EB morphology elicited by RA MS treatment, transcriptional profiling using Affymetrix GeneChip mouse genome arrays was performed in order to characterize the phenotype of the differentiating cells. RNA expression was compared between day 10 RA MS treated EBs, and EBs containing unloaded microspheres and significant gene expression changes were identified using significance analysis of microarrays (SAM) [20]. SAM analysis identified 1057 genes with a minimum threefold expression change (and $p < 0.005$), 410 of which were up-regulated in RA MS EBs, and 647

were down-regulated relative to unloaded MS EBs (Fig. 4A). Many of the genes that were up-regulated in RA MS EBs are phenotypic markers of structures specific to the early post-implantation embryo [22], including visceral endoderm, epiblast, and early primitive streak. The visceral endoderm surrounds the epiblast and provides a substrate for epiblast attachment, promotes nutrient and gas exchange, and secretes signals to direct epiblast patterning and differentiation [23,24]. The cells comprising the epiblast are pluripotent and differentiate into the entire embryo proper [25]. Primitive streak formation occurs at E6.75 in mouse embryos and is characterized by ingression of epiblast cells, which go on to form mesendodermal progenitor cells [26,27]. Visceral endoderm genes identified in the array as being significantly up-regulated in RA MS EBs included: *Dkk1* (31 fold change), *Cer1* (22), *Sox17* (20), *Hex* (18), *amnionless* (17), and *Dab2* (6.2). Epiblast-related genes up-regulated in RA MS EBs included: *Fgf5* (271), *Foxd4* (13), *Pou5f1* (aka *Oct4*, 11), *Tdgf1* (aka C*ripto1*, 6) and *Sox2* (5). Up-regulated primitive streak genes included: *Brachyury T* (195), *Eomes* (177), *Follistatin* (38), and *Mix1* (8). Genes expressed in multiple structures included: *Lhx1* (endoderm and primitive streak, 86), *Foxh1* (endoderm and epiblast, 73), *Otx2* (endoderm and epiblast, 55), and *Foxa2* (endoderm and primitive streak, 12). Other notable genes significantly up-regulated in RA MS EBs included: *Pim2* (anti-apoptosis, 785-fold change), *DNA methyltransferase 3B* (DNA methylation, 321), *cytochrome p450 family 26* (retinoic acid degradation, 74) and *laminin α1* (basement membrane, 16). Many of the genes down-regulated in RA MS EBs relative to unloaded MS EBs were related to mesoderm and definitive endoderm differentiation, including plasma proteins (albumin, transferrin, apolipoproteins, hemopexin), contractile proteins (myosin, actin and troponin), hemoglobin chains, growth factors (PDGF, VEGF, HDGF), and matrix molecules (collagen, fibronectin, vitronectin, osteopontin, versican). In summary, EBs containing unloaded microspheres exhibited reduced expression of epiblast and visceral endoderm markers and increased expression of more mature mesoderm and definitive endoderm genes, whereas treatment of EBs with RA microspheres for 10 days resulted in cystic EBs with transcriptional profiles similar to early post-implantation mouse embryos, consisting of visceral endoderm, epiblast, and early primitive streak cell phenotypes.

Temporal transcriptional analysis by quantitative PCR was performed to assess the expression of several genes found to change significantly in microarray analysis. The pluripotent transcription factor *Oct4*, expressed by cells in the inner cell mass as well as the epiblast [28], was significantly enhanced after 7 days in RA MS EBs relative to both untreated and unloaded MS EBs (Fig. 4B-i). The epiblast marker *Fgf5* was also analyzed, and in agreement with previous reports of mouse EB differentiation [29,30], untreated and unloaded MS EBs exhibited a transient increase in *Fgf5* after 2 and 4 days which subsided by day 7 (Fig. 4B-ii). In contrast, relatively high levels of *Fgf5* expression by RA MS EBs were present at 7 and 10 days of differentiation. Importantly, the pattern of *Fgf5* expression in RA MS EBs correlated with the appearance of columnar, epiblast-like cells at day 7 and completely cystic spheroids at day 10. *Brachyury T*, a transcription factor expressed in the primitive streak by mesendodermal progenitor cells [31], was also observed to transiently increase in untreated and unloaded MS EBs between days 2 and 7 of differentiation (Fig. 4B-iii). Levels of *Brachyury T* mRNA in RA MS EBs remained almost undetectable until day 10, at which point a small increase in the transcript was observed, suggesting that a subset of cells in day 10 RA MS EBs were entering the primitive streak stage. These data, together with microarray analysis, demonstrate that while EBs containing unloaded microspheres expressed markers of epiblast, primitive streak and more mature phenotypes over the course of 7 days of differentiation, RA microspheres directed EBs to form spheroids with gene expression patterns closely resembling the early post-implantation E6.75 mouse embryo.

3.5. Embryoid body immunostaining

The spatial organization of the epiblast and visceral endoderm cell populations was analyzed by immunofluorescence staining for OCT4 and FOXA2, respectively. OCT4+ cells in day 10 RA MS EBs were localized to the inner layer of columnar, pseudo-stratified cells, while the adjacent endoderm-like cells were OCT4− (Fig. 5F). The patterns of OCT4 expression were consistent for both confocal imaging of whole, permeabilized EBs and histological sections of formalin-fixed, paraffin embedded samples. In contrast, day 10 untreated and unloaded MS EBs contained regions of OCT4+ cells randomly distributed throughout the spheroid (Fig. 5D, E). Similarly, FOXA2, a marker for visceral endoderm [24], was expressed in clusters of cells dispersed throughout untreated and unloaded MS day 10 EBs (Fig. 5G, H). However in RA MS EBs, FOXA2 expression was restricted to cells in the exterior, endoderm-like layer, while cells in the epiblast-like, OCT4+ cell layer were FOXA2− (Fig. 5I). These data demonstrate that cystic RA MS EBs consist of spatially distinct populations of FOXA2+ endoderm and OCT4+ epiblast organized similar to an early streak mouse embryo.

3.6. RA MS EB ultrastructure

Embryoid bodies containing RA microspheres were examined ultrastructurally after 10 days using SEM, with micrographs displaying the two distinct epithelial layers (Fig. 6A, B). The columnar, pseudo-stratified organization of the inner layer of epiblast-like cells was readily apparent (Fig. 6B), as was the simple, squamous morphology of the overlaying endoderm layer. Interestingly, the RA MS EBs did not contain the matrix-rich outer layer observed in untreated EBs (Fig. 1B, C), but displayed a dense coat of microvilli roughly 100 nm in diameter on the exterior surface of the endodermal cell layer (Fig. 6C). These microvilli structures are similar to those that are present on the surface of visceral endoderm in days 5–7 mouse embryos [32]. Altogether, these observations demonstrate the high level of organization attained in day 10 RA MS EBs closely resembles the structural organization and phenotype of E6.75 mouse embryos.

4. Discussion

The efficient formation of highly organized, cystic EBs is significant for a number of reasons, including improved *in vitro* models of embryogenesis and biomanufacturing of differentiated cell types for regenerative medicine and *in vitro* diagnostic applications. Currently, directed differentiation strategies using EBs are limited in their ability to produce a homogeneous differentiated cell population, due largely to the fact that EBs consist of a population of cells exposed to a diverse set of instructive cues within the microenvironment [33–35]. The variability in the interactions of different cells within an EB with soluble morphogens, extracellular matrix, and neighboring cells leads to significant heterogeneity in cell differentiation microscopically within an individual EB and macroscopically among a population of EBs [36]. However, by specifying EB differentiation to two cell phenotypes initially – visceral endoderm and epiblast – it may be possible to subsequently direct cells more efficiently to specific lineages by reducing endogenous signaling, thereby allowing defined media components to more potently dictate cell fate decisions. Moreover, while untreated EBs contain a matrix-dense outer layer that appears to hinder diffusion of soluble media components, RA MS EBs contain an outer cell layer densely coated with microvilli. The appearance of microvilli strongly suggests that the outer cells may be proficient in the absorption of nutrients and soluble signaling molecules from the media, allowing such molecules to reach the interior epiblast cells more efficiently and thereby enhance subsequent directed differentiation.

The striking similarity of RA MS EBs to E6.75 embryos has significant implications for *in vitro* studies of embryogenesis. EBs have been utilized to study the roles of specific genes in development, particularly for genes in which knockout models *in vivo* are unavailable due to embryonic lethality [37,38]. However, EBs formed using conventional methods may not provide an accurate representation of the roles of such genes in later stages of embryogenesis, since EBs commonly differentiate in a heterogeneous, disorganized manner within a fairly short period of time (<7 days). The use of RA MS EBs may provide greater insight into developmental processes due to their close phenotypic resemblance to early streak (E6.75) embryos [22]. Additionally, the roles of specific secreted molecules during development can be studied in the well controlled, *in vitro* environment created using RA MS EBs, which may lead to a better understanding of early differentiation events, such as axis formation, specification of epiblast cells, and germ layer formation.

RA treatment of ESCs most commonly promotes neurogenesis [39–44]; however, enhanced cardiogenesis [45] and pancreatic beta-like cell formation [46] in response to RA have also been reported, indicating this retinol-derived morphogen is a potent inducer of differentiation to various cell lineages. Similar to the effects of RA *in vivo* [47], the concentration of RA and the timing of its delivery appear to be critical in dictating cell differentiation *in vitro* [43,48]. We report here that delivery of RA directly within the EB interior via microspheres maintains the pluripotency of ESCs through the formation of a highly organized OCT4+ epiblast, suggesting that the mode of presentation of RA (media supplement vs. microsphere-mediated) is a key determinant of cellular response, as soluble RA treatment at a wide range of concentrations [10 nM–10 μM] was unable to efficiently produce comparable cystic EBs. These discrepancies may be attributed to the fact that soluble factor delivery only affects cells at the exterior surface of EBs and prevents the remaining interior cells from being directly exposed to exogenous biochemical stimuli, such as RA. Interestingly, ESCs that constitutively express *Nodal*, a member of the TGF-β superfamily, form cystic spheroids with similar characteristics as RA MS EBs, whereas addition of recombinant Nodal to the culture media did not elicit a similar effect [49]. This suggests that 1) diffusion of Nodal into EBs is restricted and results in distinct responses between soluble delivery and constitutive local expression, and 2) the RA and TGF-β signaling pathways may share common elements [50,51], resulting in similar outcomes for local RA delivery and Nodal over-expression. Differentiation of EBs in media conditioned by HepG2 cells, a hepatocarcinoma-derived endodermal cell line, induces formation of uniform cystic EBs that lack an outer endoderm cell layer [30,52]. This suggests that in the absences of an epithelial exterior, morphogens contained within the conditioned media may more efficiently diffuse into EBs and direct differentiation. Thus, the diffusional limitations posed by EBs may be an underappreciated facet of ESC biology that may lead to an incomplete understanding of the roles of specific molecules in ESC differentiation [15].

Previous studies have reported the incorporation of PLGA microspheres containing growth factors into spheroids of fetal brain cells [16] as well as human EBs [53] in order to manipulate the biochemistry of 3D spheroid microenvironments. PLGA microspheres containing nerve growth factor (NGF) were assembled with fetal rat brain cells to form programmable neo-tissues and transplanted into adult rats. The controlled-release microspheres were able to support transplanted cell survival, but specific effects on cell differentiation were not described or compared directly to soluble delivery methods. Recently, microspheres containing angiogenic growth factors (vascular endothelial, placenta and basic fibroblast growth factors) were incorporated into EBs using forced aggregation, and expression of vascular cell markers was assessed after 10 days of differentiation. However, compared to soluble growth factor treatment, this approach did not improve vascular differentiation of human ESCs, likely due to the lack of release of growth factors after 24 h and the low overall growth factor availability. In contrast, small hydrophobic

molecules (such as RA) are readily incorporated into PLGA microspheres using a single emulsion and release is sustained over the course of days–weeks, allowing sufficient morphogen availability within EBs to elicit significant differences in ESC differentiation compared to soluble delivery methods.

5. Conclusion

Our results demonstrate that the locally controlled presentation of morphogens from microspheres-to-cells comprising an EB more closely mimics characteristics of early embryogenesis than simple soluble delivery of signaling molecules to cell spheroids. In addition to developmental studies, microsphere-mediated presentation of morphogenic cues to stem cell spheroids represents a powerful enabling technology readily capable of being integrated into bio-manufacturing strategies to obtain stem cell derivatives for regenerative medicine therapies and *in vitro* diagnostic cell technologies. Thus, the application of biomaterials and drug delivery principles to stem cell biology significantly enhances the efficiency of directed differentiation strategies and more clearly reveals the effects of specific molecules on morphogenic events.

Supplementary Material

Refer to Web version on PubMed Central for supplementary material.

Acknowledgments

We thank J. Phillips for assistance with the development of immunostaining methods and L. Matyunina for conducting microarray experiments. We are grateful to P. Ramaswami and R. Nair for assistance with manuscript preparation. This work was supported by funding from the NSF (CBET 0651739).

References

1. Evans MJ, Kaufman MH. Establishment in culture of pluripotential cells from mouse embryos. Nature 1981;292:154–6. [PubMed: 7242681]
2. Martin GR. Isolation of a pluripotent cell line from early mouse embryos cultured in medium conditioned by teratocarcinoma stem cells. Proc Natl Acad Sci U S A 1981;78:7634–8. [PubMed: 6950406]
3. Thomson JA, Itskovitz-Eldor J, Shapiro SS, Waknitz MA, Swiergiel JJ, Marshall VS, et al. Embryonic stem cell lines derived from human blastocysts. Science 1998;282:1145–7. [PubMed: 9804556]
4. Doetschman TC, Eistetter H, Katz M, Schmidt W, Kemler R. The in vitro development of blastocyst-derived embryonic stem cell lines: formation of visceral yolk sac, blood islands and myocardium. J Embryol Exp Morphol 1985;87:27–45. [PubMed: 3897439]
5. Battista S, Guarnieri D, Borselli C, Zeppetelli S, Borzacchiello A, Mayol L, et al. The effect of matrix composition of 3D constructs on embryonic stem cell differentiation. Biomaterials 2005;26:6194–207. [PubMed: 15921736]
6. Williams RL, Hilton DJ, Pease S, Willson TA, Stewart CL, Gearing DP, et al. Myeloid leukaemia inhibitory factor maintains the developmental potential of embryonic stem cells. Nature 1988;336:684–7. [PubMed: 3143916]
7. Schuldiner M, Yanuka O, Itskovitz-Eldor J, Melton DA, Benvenisty N. Effects of eight growth factors on the differentiation of cells derived from human embryonic stem cells. Proc Natl Acad Sci U S A 2000;97:11307–12. [PubMed: 11027332]
8. Ding S, Schultz PG. A role for chemistry in stem cell biology. Nat Biotechnol 2004;22:833–40. [PubMed: 15229546]
9. Hopfl G, Gassmann M, Desbaillets I. Differentiating embryonic stem cells into embryoid bodies. Methods Mol Biol 2004;254:79–98. [PubMed: 15041757]

10. Bratt-Leal AM, Carpenedo RL, McDevitt TC. Engineering the embryoid body microenvironment to direct embryonic stem cell differentiation. Biotechnol Prog. 2009 in press.
11. Brennan J, Lu CC, Norris DP, Rodriguez TA, Beddington RS, Robertson EJ. Nodal signalling in the epiblast patterns the early mouse embryo. Nature 2001;411:965–9. [PubMed: 11418863]
12. Niederreither K, Vermot J, Schuhbaur B, Chambon P, Dolle P. Retinoic acid synthesis and hindbrain patterning in the mouse embryo. Development 2000;127:75–85. [PubMed: 10654602]
13. Chiang C, Litingtung Y, Lee E, Young KE, Corden JL, Westphal H, et al. Cyclopia and defective axial patterning in mice lacking Sonic hedgehog gene function. Nature 1996;383:407–13. [PubMed: 8837770]
14. Winnier G, Blessing M, Labosky PA, Hogan BL. Bone morphogenetic protein-4 is required for mesoderm formation and patterning in the mouse. Genes Dev 1995;9:2105–16. [PubMed: 7657163]
15. Sachlos E, Auguste DT. Embryoid body morphology influences diffusive transport of inductive biochemicals: a strategy for stem cell differentiation. Biomaterials 2008;29:4471–80. [PubMed: 18793799]
16. Mahoney MJ, Saltzman WM. Transplantation of brain cells assembled around a programmable synthetic microenvironment. Nat Biotechnol 2001;19:934–9. [PubMed: 11581658]
17. Richardson TP, Peters MC, Ennett AB, Mooney DJ. Polymeric system for dual growth factor delivery. Nat Biotechnol 2001;19:1029–34. [PubMed: 11689847]
18. Jeong YI, Song JG, Kang SS, Ryu HH, Lee YH, Choi C, et al. Preparation of poly (DL-lactide-*co*-glycolide) microspheres encapsulating all-trans retinoic acid. Int J Pharm 2003;259:79–91. [PubMed: 12787638]
19. Carpenedo RL, Sargent CY, McDevitt TC. Rotary suspension culture enhances the efficiency, yield, and homogeneity of embryoid body differentiation. Stem Cells 2007;25:2224–34. [PubMed: 17585171]
20. Tusher VG, Tibshirani R, Chu G. Significance analysis of microarrays applied to the ionizing radiation response. Proc Natl Acad Sci U S A 2001;98:5116–21. [PubMed: 11309499]
21. Niederreither K, Subbarayan V, Dolle P, Chambon P. Embryonic retinoic acid synthesis is essential for early mouse post-implantation development. Nat Genet 1999;21:444–8. [PubMed: 10192400]
22. Pfister S, Steiner KA, Tam PP. Gene expression pattern and progression of embryogenesis in the immediate post-implantation period of mouse development. Gene Expr Patterns 2007;7:558–73. [PubMed: 17331809]
23. Bielinska M, Narita N, Wilson DB. Distinct roles for visceral endoderm during embryonic mouse development. Int J Dev Biol 1999;43:183–205. [PubMed: 10410899]
24. Dufort D, Schwartz L, Harpal K, Rossant J. The transcription factor HNF3beta is required in visceral endoderm for normal primitive streak morphogenesis. Development 1998;125:3015–25. [PubMed: 9671576]
25. Lawson KA, Meneses JJ, Pedersen RA. Clonal analysis of epiblast fate during germ layer formation in the mouse embryo. Development 1991;113:891–911. [PubMed: 1821858]
26. Burdsal CA, Damsky CH, Pedersen RA. The role of E-cadherin and integrins in mesoderm differentiation and migration at the mammalian primitive streak. Development 1993;118:829–44. [PubMed: 7521282]
27. Ciruna BG, Schwartz L, Harpal K, Yamaguchi TP, Rossant J. Chimeric analysis of fibroblast growth factor receptor-1 (Fgfr1) function: a role for FGFR1 in morphogenetic movement through the primitive streak. Development 1997;124:2829–41. [PubMed: 9226454]
28. Palmieri SL, Peter W, Hess H, Scholer HR. Oct-4 transcription factor is differentially expressed in the mouse embryo during establishment of the first two extraembryonic cell lineages involved in implantation. Dev Biol 1994;166:259–67. [PubMed: 7958450]
29. Bruce SJ, Gardiner BB, Burke LJ, Gongora MM, Grimmond SM, Perkins AC. Dynamic transcription programs during ES cell differentiation towards mesoderm in serum versus serum-freeBMP4 culture. BMC Genomics 2007;8:365. [PubMed: 17925037]

30. Rathjen J, Haines BP, Hudson KM, Nesci A, Dunn S, Rathjen PD. Directed differentiation of pluripotent cells to neural lineages: homogeneous formation and differentiation of a neurectoderm population. Development 2002;129:2649–61. [PubMed: 12015293]
31. Rivera-Perez JA, Magnuson T. Primitive streak formation in mice is preceded by localized activation of Brachyury and Wnt3. Dev Biol 2005;288:363–71. [PubMed: 16289026]
32. Ishikawa T, Yagyu K, Seguchi H. A scanning electron microscopic study of the surface morphology of visceral endoderm and ectoderm in postimplantation mouse embryos. J Electron Microsc (Tokyo) 1986;35:185–94. [PubMed: 3572293]
33. Itskovitz-Eldor J, Schuldiner M, Karsenti D, Eden A, Yanuka O, Amit M, et al. Differentiation of human embryonic stem cells into embryoid bodies compromising the three embryonic germ layers. Mol Med 2000;6:88–95. [PubMed: 10859025]
34. Li M, Pevny L, Lovell-Badge R, Smith A. Generation of purified neural precursors from embryonic stem cells by lineage selection. Curr Biol 1998;8:971–4. [PubMed: 9742400]
35. O'Shea KS. Neuronal differentiation of mouse embryonic stem cells: lineage selection and forced differentiation paradigms. Blood Cells Mol Dis 2001;27:705–12. [PubMed: 11482885]
36. Metallo CM, Mohr JC, Detzel CJ, de Pablo JJ, Van Wie BJ, Palecek SP. Engineering the stem cell microenvironment. Biotechnol Prog 2007;23:18–23. [PubMed: 17269664]
37. Li X, Chen Y, Scheele S, Arman E, Haffner-Krausz R, Ekblom P, et al. Fibroblast growth factor signaling and basement membrane assembly are connected during epithelial morphogenesis of the embryoid body. J Cell Biol 2001;153:811–22. [PubMed: 11352941]
38. Quinn G, Ochiya T, Terada M, Yoshida T. Mouse flt-1 promoter directs endothelial-specific expression in the embryoid body model of embryogenesis. Biochem Biophys Res Commun 2000;276:1089–99. [PubMed: 11027595]
39. Bain G, Kitchens D, Yao M, Huettner JE, Gottlieb DI. Embryonic stem cells express neuronal properties in vitro. Dev Biol 1995;168:342–57. [PubMed: 7729574]
40. Bain G, Ray WJ, Yao M, Gottlieb DI. Retinoic acid promotes neural and represses mesodermal gene expression in mouse embryonic stem cells in culture. Biochem Biophys Res Commun 1996;223:691–4. [PubMed: 8687458]
41. Fraichard A, Chassande O, Bilbaut G, Dehay C, Savatier P, Samarut J. In vitro differentiation of embryonic stem cells into glial cells and functional neurons. J Cell Sci 1995;108:3181–8. [PubMed: 7593279]
42. Irioka T, Watanabe K, Mizusawa H, Mizuseki K, Sasai Y. Distinct effects of caudalizing factors on regional specification of embryonic stem cell-derived neural precursors. Brain Res Dev Brain Res 2005;154:63–70.
43. Okada Y, Shimazaki T, Sobue G, Okano H. Retinoic-acid-concentration-dependent acquisition of neural cell identity during in vitro differentiation of mouse embryonic stem cells. Dev Biol 2004;275:124–42. [PubMed: 15464577]
44. Pachernik J, Bryja V, Esner M, Kubala L, Dvorak P, Hampl A. Neural differentiation of pluripotent mouse embryonal carcinoma cells by retinoic acid: inhibitory effect of serum. Physiol Res 2005;54:115–22. [PubMed: 15717849]
45. Hidaka K, Lee JK, Kim HS, Ihm CH, Iio A, Ogawa M, et al. Chamber-specific differentiation of Nkx2.5-positive cardiac precursor cells from murine embryonic stem cells. FASEB J 2003;17:740–2. [PubMed: 12594186]
46. Micallef SJ, Janes ME, Knezevic K, Davis RP, Elefanty AG, Stanley EG. Retinoic acid induces Pdx1-positive endoderm in differentiating mouse embryonic stem cells. Diabetes 2005;54:301–5. [PubMed: 15585742]
47. White RJ, Nie Q, Lander AD, Schilling TF. Complex regulation of cyp26a1 creates a robust retinoic acid gradient in the zebrafish embryo. PLoS Biol 2007;5:e304. [PubMed: 18031199]
48. Goncalves MB, Boyle J, Webber DJ, Hall S, Minger SL, Corcoran JP. Timing of the retinoid-signalling pathway determines the expression of neuronal markers in neural progenitor cells. Dev Biol 2005;278:60–70. [PubMed: 15649461]
49. Vallier L, Reynolds D, Pedersen RA. Nodal inhibits differentiation of human embryonic stem cells along the neuroectodermal default pathway. Dev Biol 2004;275:403–21. [PubMed: 15501227]

50. Cao Z, Flanders KC, Bertolette D, Lyakh LA, Wurthner JU, Parks WT, et al. Levels of phospho-Smad2/3 are sensors of the interplay between effects of TGF-beta and retinoic acid on monocytic and granulocytic differentiation of HL-60 cells. Blood 2003;101:498–507. [PubMed: 12393416]

51. Pendaries V, Verrecchia F, Michel S, Mauviel A. Retinoic acid receptors interfere with the TGF-beta/Smad signaling pathway in a ligand-specific manner. Oncogene 2003;22:8212–20. [PubMed: 14603262]

52. Rathjen J, Lake JA, Bettess MD, Washington JM, Chapman G, Rathjen PD. Formation of a primitive ectoderm like cell population, EPL cells, from ES cells in response to biologically derived factors. J Cell Sci 1999;112(Pt 5):601–12. [PubMed: 9973595]

53. Ferreira L, Squier T, Park H, Choe H, Kohane DS, Langer R. Human embryoid bodies containing nano- and microparticulate delivery vehicles. Adv Mater 2008;20:2285–91.

Appendix

Figures with essential colour discrimination. Certain parts of the majority of the figures in this article are difficult to interpret in black and white. The full colour images can be found in the on-line version, atdoi:10.1016/j.biomaterials.2009.01.007.

Appendix. Supplementary material

Supplementary data associated with this article can be found, in the online version, at doi: 10.1016/j.biomaterials.2009.01.007.

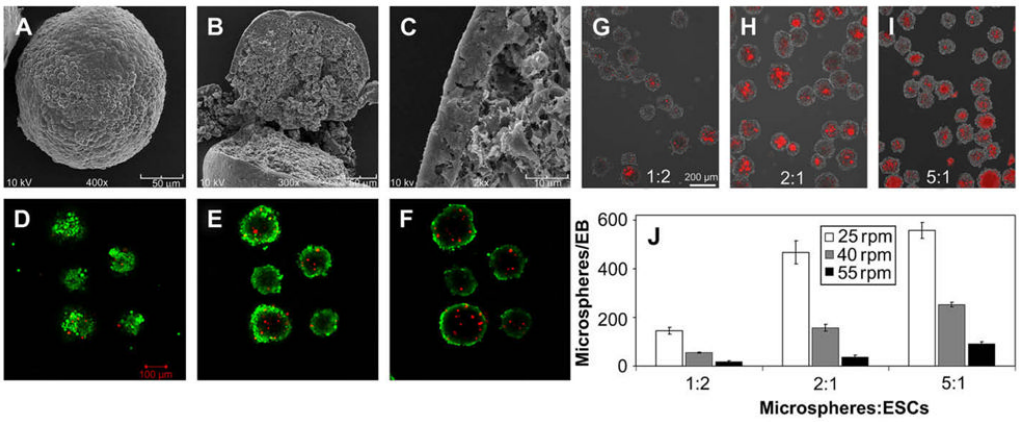

Fig. 1.

EB structure and microsphere incorporation. (A) Day 10 EBs exhibited a smooth exterior in SEM micrographs, while bisected EBs displayed a dense outer layer (B, C). (D–F), Microspheres labeled with CellTracker Red were observed in multiple focal planes (30 μm between images), while soluble treatment of CellTracker Green labeled the outermost 1–2 cell layers. (G–I) EBs formed at 40 rpm with 1:2 (G), 2:1 (H) and 5:1 (I) ratios of CellTracker Red microspheres-to-cells displayed increasing levels of microsphere incorporation. (J) Quantification of microsphere incorporation in populations of lysed EBs demonstrated that lower rotary speed and higher microsphere to cell ratios increased microsphere incorporation (n = 3, mean ± standard deviation).

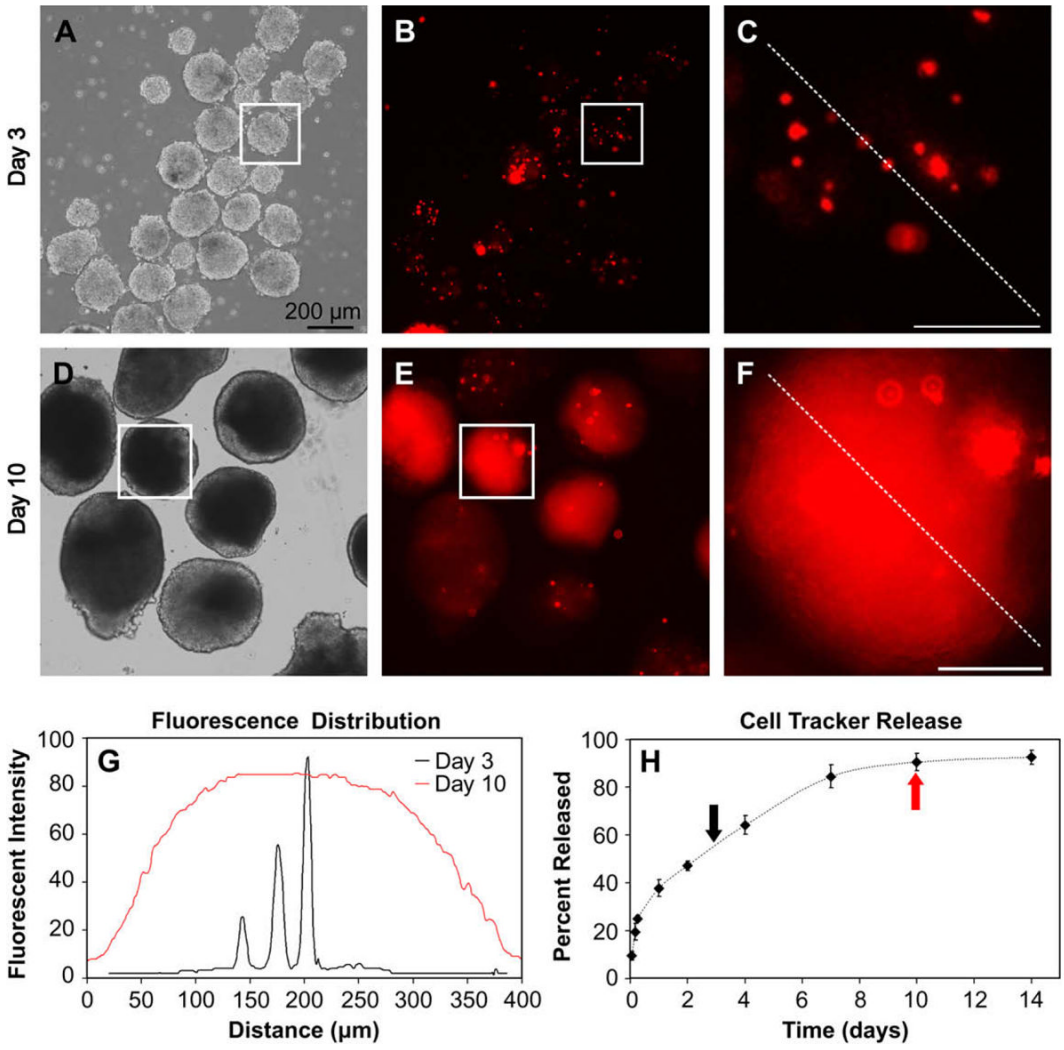

Fig. 2.

Small molecule release within EBs. EBs formed at 40 rpm with a 2:1 microsphere to cell ratio were imaged after 3 (A–C) and 10 days (D–F). (A–C) After 3 days, microspheres were visible within EBs as individual, punctuate spheres. (D–F) EBs imaged after 10 days contained diffuse fluorescence throughout and fewer individual spheres were apparent. (G) Fluorescent intensity plots across day 3 and day 10 EBs (dashed lines in C and F, respectively) revealed the presence of individual microspheres in day 3 EBs and uniform fluorescence throughout day 10 EBs. (H) CellTracker was released from microspheres over the course of 14 days, and a burst phase (up to one day), sustained release phase (1–7 days), and plateau phase (7–14 days) were observed (n = 3, mean ± standard deviation). (A, B, D, E bar = 200 μm; C, F bar = 100 μm).

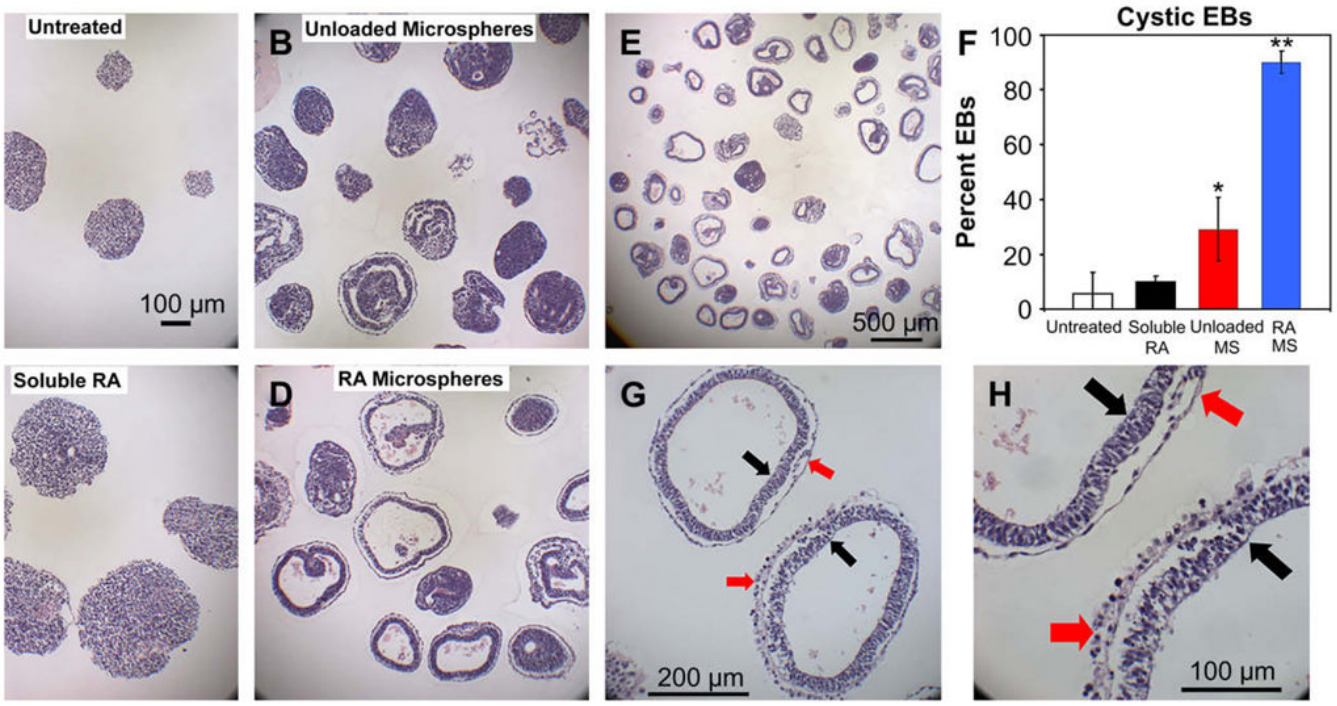

Fig. 3.

Delivery of retinoic acid to EBs. Untreated EBs as well as EBs treated with soluble RA, unloaded microspheres, or RA-loaded microspheres were formalin-fixed, sectioned and stained with H&E after 10 days of differentiation. (A) Untreated EBs and (C) soluble RA treated EBs formed solid spheroids while (B) EBs containing unloaded microspheres contained small void spaces. (D, E) EBs containing RA microspheres frequently were completely cystic. (F) Cystic EB formation was significantly enhanced in RA MS EBs compared to all other treatments (n = 3, mean ± standard deviation). (G, H) Cystic RA MS EBs contained bi-epithelial morphology, with a columnar, pseudo-stratified inner cell layer (black arrows) and an adjacent, flattened outermost cell layer (red arrows). *Denotes $p < 0.05$ vs. untreated, soluble RA; **denotes $p = 6 \times 10^{-6}$ vs. all treatments.

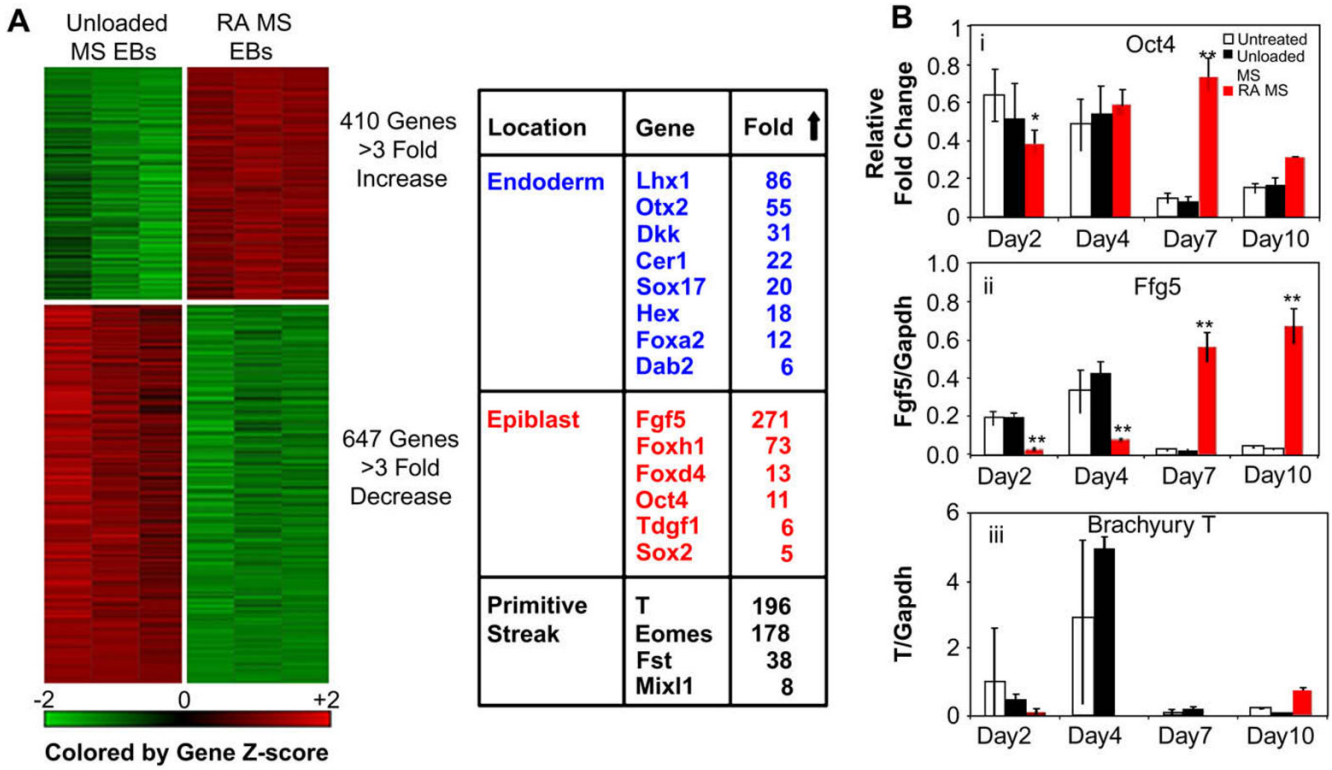

Location	Gene	Fold
Endoderm	Lhx1	86
	Otx2	55
	Dkk	31
	Cer1	22
	Sox17	20
	Hex	18
	Foxa2	12
	Dab2	6
Epiblast	Fgf5	271
	Foxh1	73
	Foxd4	13
	Oct4	11
	Tdgf1	6
	Sox2	5
Primitive Streak	T	196
	Eomes	178
	Fst	38
	Mixl1	8

Fig. 4.

Gene expression analysis. Transcriptional analysis of EBs was performed using GeneChip microarrays (A) and quantitative PCR (B). (A) 410 genes were identified as up-regulated greater than threefold in RA microsphere EBs compared to unloaded microsphere EBs after 10 days of differentiation, while 647 genes were observed to decrease in RA MS EBs. Many genes with large fold changes in RA MS EBs were associated with early embryonic structures, including visceral endoderm, epiblast and primitive streak. (B) Time course quantitative PCR analysis of i) *Oct4*, ii) *Fgf5*, and iii) *Brachyury T* gene expression. The epiblast markers *Oct4* and *Fgf5* were significantly enhanced in RA MS EBs after 7 days, and *Fgf5* was enhanced after 10 days as well. Expression of *Brachyury T*, a marker for primitive streak, in RA MS EBs was delayed until day 10, when a small increase was observed ($n = 3$, mean ± standard deviation). *Denotes $p = 0.02$ vs. untreated; **denotes $p < 0.05$ vs. all treatments; ***denotes $p = 5.2 \times 10^{-6}$ vs. all treatments.

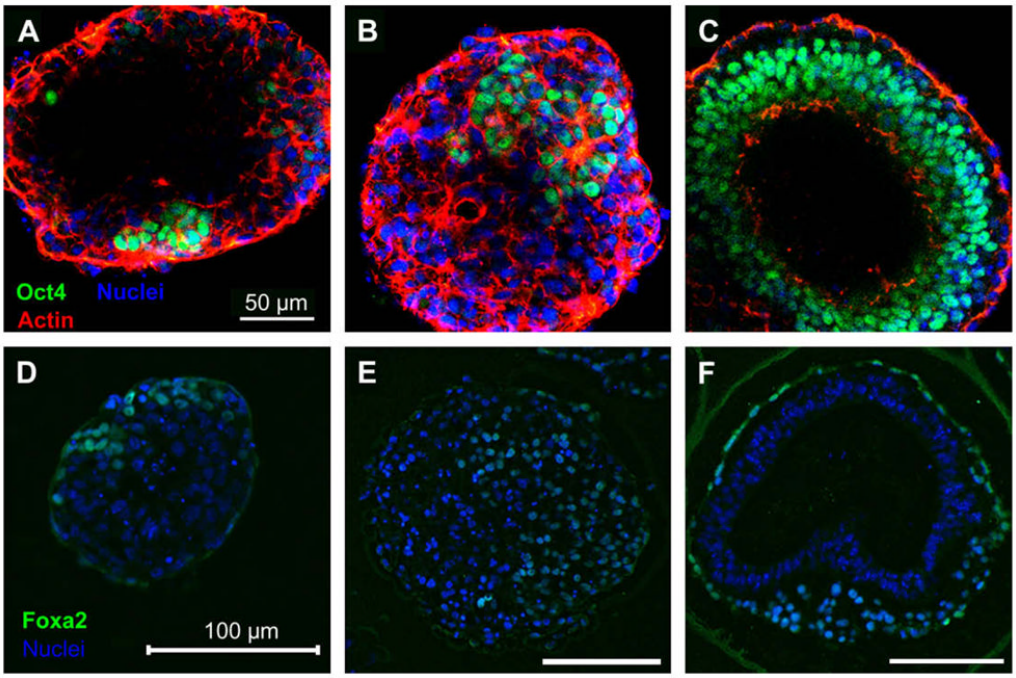

Fig. 5.

Immunostaining of EBs. (A–C) OCT4 staining was performed on day 10 untreated (A), unloaded MS (B) and RA MS EBs (C). Untreated and unloaded MS EBs contained clusters of OCT4+ cells, while OCT4+ cells in RA MS EBs were localized to the columnar cell layer. (D–E) FOXA2, a marker of visceral endoderm, was also expressed in clusters of untreated (D) and unloaded MS EBs (E), but was localized to the outermost layer of cell in RA MS EBs (F). A–C, bar = 50 μm; D–F, bar = 100 μm.

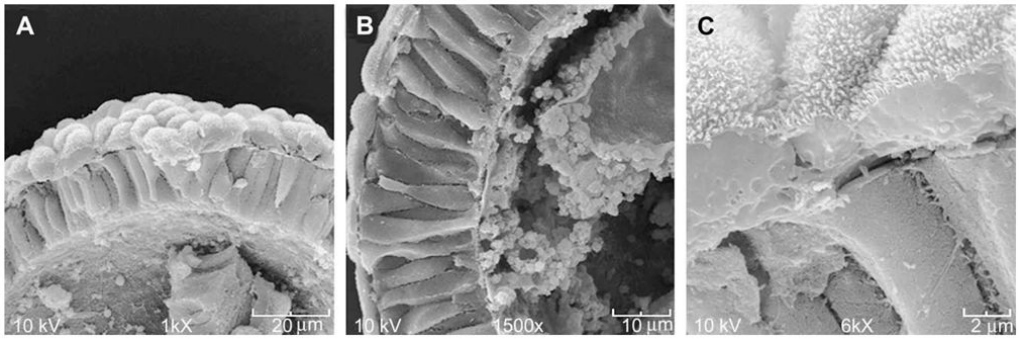

Fig. 6.

RA MS EB ultrastructure. (A, B) SEM micrographs of day 10 RA MS EBs reveal the structure of the distinct squamous endoderm and pseudo-stratified epiblast layers. (C) A dense coat of microvilli were observed on the surface of the endoderm cells, similar to that observed on early streak stage mouse embryos.